Zhang, X., **Yang, X.**, **Jomaa, S.**, **Rode, M.** (2020):
Analyzing impacts of seasonality and landscape gradient on event-scale nitrate-discharge dynamics based on nested high-frequency monitoring
J. Hydrol. **591** , art. 125585

http://dx.doi.org/10.1016/j.jhydrol.2020.125585

Analyzing impacts of seasonality and landscape gradient on event-scale nitrate-discharge dynamics based on nested high-frequency monitoring

Xiaolin Zhang[1,*], Xiaoqiang Yang[1, 2,*], Seifeddine Jomaa[1], Michael Rode[1]

[1]Helmholtz Centre for Environment Research - UFZ, Department of Aquatic Ecosystem Analysis and Management, Magdeburg, Germany

[2]Department of Ecohydrology, Leibniz Institute of Freshwater Ecosystem and Inland Fisheries, Berlin, Germany

(*xiaolin.zhang@ufz.de, *xiaoqiang.yang@ufz.de, seifeddine.jomaa@ufz.de, michael.rode@ufz.de)

Highlights

- Spatial heterogeneity of nitrate storage can affect patterns of C-Q relationships
- Hydrological connectivity on land determined seasonally varying nitrate exports
- Nested monitoring is needed to explore C-Q mechanisms in heterogeneous catchments
- Analysis of C-Q hysteresis pattern allow targeting agricultural management actions

Abstract

Increasingly available high-frequency data during storm events, when hydrological dynamics most likely activate nitrate storage-flux exchanges, reveal insights into catchment nitrate dynamics. In this study, we explored impacts of seasonality and landscape gradients on nitrate concentration-discharge (C-Q) hysteresis patterns in the Selke catchment, central Germany, which has heterogeneous combinations of meteorological, hydrogeological and land use conditions. Three nested gauging stations established along the main Selke River captured flow and nitrate export dynamics from the uppermost subcatchment (mixed forest and arable land), middle subcatchment (pure steep forest) and lowermost subcatchment (arable and urban land). We collected continuous high-frequency (15-min) discharge and nitrate concentration data from 2012-2017 and analyzed the 223 events detected at all three stations. A dominant hysteresis pattern in the uppermost and middle subcatchments was counter-clockwise and combined with an accretion effect, indicating many proximal and mobilized distal nitrate sources. However, 66% of all events at the catchment outlet experienced a dilution effect, possibly due to mechanisms that vary seasonally. During wetting/wet periods (October-March), it was combined mainly with a counter-clockwise pattern due to the dominance of event runoff volume from the uppermost and middle subcatchments. During drying/dry periods (April-September), however, it was combined mainly with a clockwise pattern due to occasional quick surface flows from lowland near-stream urban areas. In addition, the clockwise hysteresis occurred mainly from May-October during mostly drying/dry periods at all three sites, indicating little distal nitrate transport in response to the low terrestrial hydrological connectivity, especially in the lowermost dry and flat subcatchment. This comprehensive analysis (i.e., clockwise vs. counter-clockwise, accretion vs. dilution) enables in-depth analysis of nitrate export mechanisms during certain periods under different landscape conditions. Specific combination of C-Q relationships could identify target locations for agricultural management actions that decrease nitrate output. Therefore, we strongly encourage long-term multisite and high-frequency monitoring strategies in heterogeneous nested catchment(s), which can help understand process mechanisms, generate data for physical-based water-quality modeling and provide guidance for water and agricultural management.

Key words: nitrate export dynamic, C-Q relationship, hysteresis pattern, high-frequency data, landscape effect, seasonality effect

1. Introduction

Human activities (e.g., intensive agriculture, urbanization, deforestation) have altered the natural landscape extensively and hence influenced nitrogen (N) cycling greatly (Boyer et al., 2002; Howarth et al., 2012). The large external supplies of N clearly exceed terrestrial N demands for plant/crop growth and microbial transformation (Davidson et al., 2011). Driven by hydrological dynamics, the excess terrestrial N has been exported to surface waters and redistributed spatially and temporally throughout fresh/coastal water systems (Reusch et al., 2018; Shields et al., 2008). Mitigation measures have been established according to guidelines of multiple government conventions (e.g., the European Union Water Framework Directive). Although diffuse nitrate pollution has been ameliorated, it remains a main cause of freshwater quality degradation (EEA, 2018). Pursuing more cost-effective measures requires better mechanistic understanding of catchment nitrate dynamics, especially in the context of contrasting landscape conditions (both natural and human) and strong seasonal variability.

Flow and nitrate dynamics during storm events are more active due to changes in storage-flux interactions and transport pathways, compared to those during hydrologically stable conditions (e.g., low flow, dry periods). Therefore, the event-scale relationship between nitrate concentration and discharge (C-Q relationship) has been investigated intensively to determine spatial and temporal variability in catchment nitrate functioning (Baker and Showers, 2019; Dupas et al., 2016; Zimmer et al., 2019). Hysteresis is the most commonly observed pattern of the C-Q relationship (Burns et al., 2019). Hysteresis patterns vary spatially and temporally due to variable combinations of nitrate sources (Bowes et al., 2015) and hydrological drivers (Vaughan et al., 2017). Celerity is well known to be faster than particle transport velocity in catchment hydrology (Cheraghi et al., 2016; McDonnell and Beven, 2014; Williams et al., 2018). Therefore, proximal nitrate storages generally respond faster than distal storages along the formation of hydrograph at the catchment scale, resulting in different hysteresis loops of the C-Q relationship (i.e., clockwise vs counter-clockwise). Meanwhile, nitrate storage varies vertically (along the soil profile) and horizontally under different landscape characteristics and anthropogenic conditions (Dupas et al., 2016; Musolff et al., 2016; Miller et al., 2017). Driven by flow generations, the mobilized terrestrial nitrate may further result in negative or positive hysteresis slopes for stream water, representing dilution or accretion effects, respectively. In turn, hysteresis analysis based on comprehensive monitoring data permits detailed explorations of the varying flow and nitrate dynamics. Continuous high-frequency data under various hydro-climatic conditions offers the opportunity to evaluate the changes of runoff partitioning and biogeochemical processes, as well as their impacts on nitrate mobilizations at multiple spatial scales (e.g., for the catchment-wide scale and the local near stream scale) (Carey et al., 2014; Vaughan et al., 2017). Intensive monitoring across contrasting landscape characteristics further enables detailed analysis of the interplay between heterogeneous landscape features and varying flow pathways (Fovet et al., 2018; Musolff et al., 2015; Williams et al., 2018).

Landscape characteristics reflect regional climate patterns, general pedological and geological properties and human impacts. Therefore, the spatial heterogeneity of landscape characteristics determines the spatial distribution of nitrate source areas and variable catchment mechanisms of hydrology and nutrient transport (Dupas et al., 2017; Poor and McDonnell, 2007). The long history of commercial fertilizer application has increased agricultural production but has also accumulated excess N in terrestrial soils (Outram et al., 2016). N sources from agricultural lands have become one of the main pollution sources in most rivers and caused high risks to aquatic ecosystems (EEA, 2019). In forest areas, nitrate leaching likely depends on the amount of nitrate in throughfall and the C:N ratio of the organic soil horizon (Borken and Matzner, 2004; MacDonald et al., 2002). Therefore, a synchronous dynamic pattern between discharge and nitrate concentration is commonly observed in forest catchments. Artificial N is added mainly via atmospheric wet and dry deposition (e.g., ranging from 1-60 kg N ha^{-1} yr^{-1}), which has also been increased greatly in the past few decades (MacDonald et al., 2002). In urban areas, extensive paved areas and artificial drainage networks can strongly alter natural processes of water movement and nitrate transport (Miller et al., 2014). For example, artificially drained flow easily bypasses the nitrate-rich soil and responds quickly, even under small precipitation events. Therefore, the process of N export can be misunderstood if the heterogeneity of catchment landscape characteristics is not considered, especially in nonuniform and nested catchments.

Driven by seasonal variations in meteorological and hydrological conditions, terrestrial export of nitrate always accompanies the changes of runoff components, and therefore, the surface nitrate C-Q relationship shows strong seasonality (Sickman et al., 2003). Different runoff components (i.e., surface flow, interflow and baseflow) usually have different nitrate concentrations due to their differing degrees of interactions with soil N sources (Miller et al., 2017). Therefore, the seasonally varying characteristic of runoff partitioning can alter the C-Q relationship of specific events considerably. Recent researches about C-Q relationship most focus on humid areas (Jacobs et al., 2018; Vaughan et al., 2017; Zimmer et al., 2019), where interflow plays an important role in transporting nitrate sources during events. Studies of process-based understanding of temporal nitrate dynamics in dry area are still rare (Dupas et al., 2016). For example, interflow and baseflow are considered the dominant runoff components during wet and dry periods, respectively, in the well-monitored Selke catchment in central Germany (Yang et al., 2018). However, quick surface flow from paved area and artificial drainage (both with relatively low nitrate concentrations) can also occur intermittently in the lowland arable/urban area during small events and cause different C-Q relationships at the outlet. The interplay among different runoff components and their effects on nitrate dynamics in dry area are hence in need of improved understanding. Moreover, seasonal biogeochemical processes can also influence the nitrate legacy at the catchment scale. In Western Europe, winter-spring high-flow periods experience high soil moisture, which activates hydrological connections between terrestrial and aquatic systems (Molenat et al., 2008; Strohmenger et al., 2020), and relatively low temperatures, which do not stimulate much biogeochemical turnover (Allen et al., 2002). In contrast, summer-autumn high-temperature growing seasons cause high soil evaporation and plant/crop transpiration, which result in low soil moisture that restricts hydrological connections (Bracken and Croke, 2007) and stimulates biogeochemical transformations of N in terrestrial and in-stream phases (Racchetti et al., 2011; Rode et al., 2016a). Hence, these seasonal hydrological and biogeochemical processes can characterize the variation in the C-Q relationship.

Overall, the mechanistic interactions between flow and nitrate dynamics at the event scale vary spatially and temporally. Comprehensive monitoring datasets for highly heterogeneous catchments are rare, but they are essential to reveal effects of landscape heterogeneity and seasonality on C-Q relationships. In this study, we focused on the well-monitored Selke catchment (a subcatchment of the Terrestrial Environmental Observatories (TERENO) – Harz/Central German Lowland Observatory) (Wollschläger et al., 2016; Zacharias et al., 2011). Three nested gauging stations along the main Selke River capture the variety of catchment responses of flow and nitrate processes (Jiang et al., 2019; Yang et al., 2018). High-frequency multi-parameter sensors have been continuously deployed at each station, ranging from upper forest area to lowland agricultural area (Rode et al., 2016a). Here we collected discharge and nitrate-N concentration data that were continuously monitored during 2012-2017 at a 15-min interval. The objectives of this study were to (1) quantify event-scale C-Q relationships among heterogeneous conditions in the nested Selke catchment, (2) analyze impacts of deviating hydrological and landscape characteristics on hysteresis patterns based on subcatchments discrepancies, and (3) investigate seasonal variability of hysteresis patterns given the contrasting wet-dry conditions. With this study we show how nitrate fluxes are generated in heterogeneous subcatchments and how the interplay of these subcatchments can modulate C-Q relationships at varying seasonal conditions and event magnitudes at the whole catchment scale.

2. Data and methods

2.1. Study area and data collection

The Selke catchment (456 km^2) is located in the transition area between the northern German plain and central German uplands. The elevation ranges from ca. 590 m in the upper Harz mountain region to ca. 100 m in the lowland region (Figure 1a), with mean annual precipitation decreasing from 790 to 450 mm, respectively (Yang et al., 2019). Three gauging stations set up from upstream to downstream (i.e., Silberhuette (SILB), Meisdorf (MEIS) and Hausneindorf (HAUS)) (Figure 1a) capture responses of the heterogeneous catchments (Rode et al., 2016a). The drainage areas of the three stations are 99, 184, and 456 km^2, respectively. The uppermost and middle subcatchments lie in the Harz mountainous region, which is dominated by shallow and relatively impervious schist and claystone overlain mainly by cambisols. In contrast, the lowermost subcatchment lies in the unique central German loess-chernozem region, which has deep tertiary sedimentary rocks. Therefore, the catchment has high gradients of landscape characteristics, including meteorology, hydrology, biogeochemistry and anthropogenic impacts (Yang et al., 2019). The uppermost subcatchment is covered by well-mixed forest (60%) and agricultural (25%) areas, while most (85%) of the middle subcatchment is covered by pure steep forest (Figure 1b). Due to the high fertility of chernozems, the lowermost subcatchment is extensively and intensively cultivated as arable land (ca. 80%) and contains considerable urban areas.

Both discharge and nitrate-N ($NO_3^- - N$) concentration are continuously measured at the three gauging stations. We collected high-frequency (15-min interval) data from 2012-2017 for the event-scale analysis. Discharge data were provided by the State Agency for Flood Protection and Water Management of Saxony-Anhalt (LHW). $NO_3^- - N$ data were provided by the Helmholtz Center for Environmental Research-UFZ, using a TRIOS ProPS-UV sensor with an optical path length of 10 mm. The sensor data were validated by biweekly parallel grab samples. For more information about the high-frequency monitoring and maintenance, please refer to Rode et al. (2016b). In addition, long-term daily discharge and biweekly grab-sampled $NO_3^- - N$ data (1994 - 2011) from LHW were also collected for a long-term overview of flow and $NO_3^- - N$ concentration dynamics.

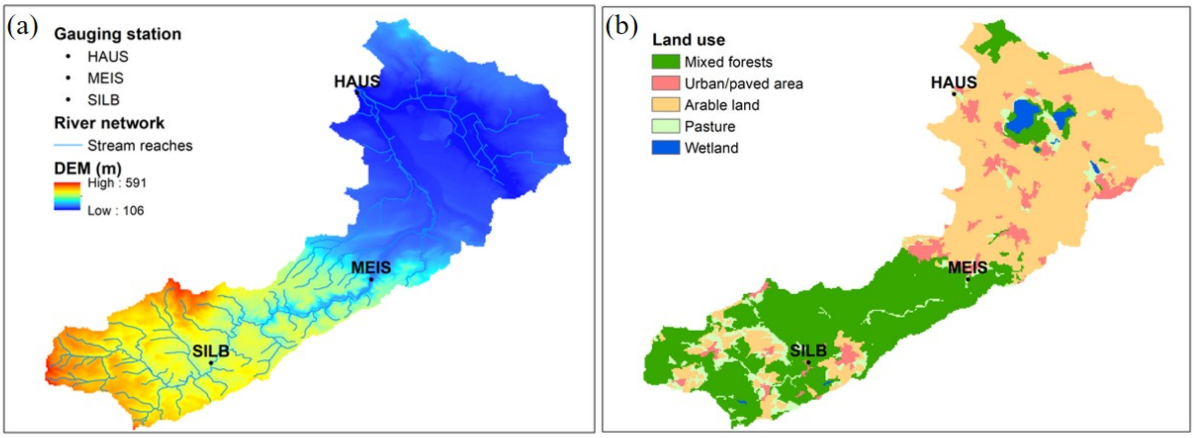

Figure 1. (a) Elevation and (b) land use in the Selke catchment and locations of the three gauging stations.

2.2. Variability in event-scale nitrate dynamics

2.2.1. Detecting storm events

Storm events were detected first based on automatic identification of all local maxima and minima of the discharge time series. Each local maximum was considered to be the discharge peak of each event, and the closest minima before and after the peak were selected as the preliminary start- and end-time of the event, respectively. Next, the final start- and end-times of each event were manually adjusted to ensure that they had a similar discharge. Successive events without a complete recession between them were merged into a single event with multiple peaks. Events with missing data (> 10%) were excluded from further analysis. Events were detected using scripts in R software (R Core Team, 2020).

2.2.2. Calculation of hysteresis patterns

For each event, discharge and $NO_3^- - N$ were normalized following Lloyd et al. (2016a):

$$Q_{t,norm} = \frac{Q_t - Q_{min}}{Q_{max} - Q_{min}} \tag{1}$$

$$N_{t,norm} = \frac{N_t - N_{min}}{N_{max} - N_{min}} \tag{2}$$

where Q_t and N_t are the discharge (m^3 s^{-1}) and $NO_3^- - N$ (mg l^{-1}) concentration measured at time *t*, $Q_{t,norm}$ and $N_{t,norm}$ are the normalized discharge and $NO_3^- - N$ concentration, and the subscripts '$_{min}$' and '$_{max}$' are the minimum and maximum values of each event.

To quantify the hysteresis pattern of the C-Q relationship, two indices were calculated from the normalized data. First, the non-dimensional hysteresis index (*HI*) was calculated as:

$$HI = \int N_{t,norm} \cdot dQ_{t,norm} \quad (3)$$

where *HI* equals the sum of hysteresis effects of the C-Q relationship during each event period (Zhang et al., 2017). *HI* ranges from -1 to 1 ($HI > 0$ indicates clockwise hysteresis, while $HI < 0$ indicates counter-clockwise hysteresis). Second, the concentration-changed index (*CI*), following Butturini et al. (2008), was calculated as:

$$CI = N_{tp,norm} - N_{ts,norm} \quad (4)$$

where $N_{tp,norm}$ and $N_{ts,norm}$ are the normalized $NO_3^- - N$ concentration at the discharge peak and start-time of each event, respectively. *CI* ranges from -1 to 1 ($CI > 0$ indicates an accretion effect of $NO_3^- - N$ concentration following flow dynamics, while $CI < 0$ indicates a dilution effect). Note that if the peak discharge lasted for more than one measured time point, the first time point $NO_3^- - N$ concentration was chosen as $N_{tp,norm}$.

2.2.3. Shared event analysis and statistic methods

Several "shared events" were specifically analyzed based on the start-, end- and discharge peak time points of each event at the SILB, MEIS, and HAUS stations. These events propagated from upstream to downstream and were detected simultaneously at all three stations. Then, the start- and end-times of each shared event were adjusted slightly to encompass the entire event duration at all three stations (i.e., using the latest start-time and the earliest end-time). Nitrate-N load (N_L, unit: kg) and runoff volume (R_V, unit: m^3) of each shared event at each station were calculated using the following two equations, respectively:

$$N_L = \int (Q_t \cdot N_t) \cdot dt \quad (5)$$

$$R_V = \int Q_t \cdot dt \quad (6)$$

where Q_t and N_t are the measured discharge (m^3 s^{-1}) and $NO_3^- - N$ concentration (mg l^{-1}), respectively, during the shared period. Using values of N_L and R_V from the three nested stations, nitrate-N load and runoff volume were calculated for the uppermost subcatchment (subscript '$_{UP}$') as the values measured at the SILB station, for the middle subcatchment (subscript '$_{MID}$') as the values measured at the MEIS station minus those at the SILB station and for the lowermost subcatchment (subscript '$_{LOW}$') as the values measured at the HAUS station minus those at the MEIS station. In addition, nitrate-N load and runoff volume of the entire catchment (subscript '$_{ALL}$') were considered as the values measured at the HAUS station.

The nonparametric Wilcoxon signed rank test and Kruskal-Wallis test were used to detect significant differences in population medians of paired or multiple categories, respectively (Kruskal and Wallis, 1952; Wilcoxon, 1945). The distributions of samples were considered significantly different when the *p*-value was below the level of significance of 0.05.

3. Results

3.1. Overview of long-term dynamics

In the long-term data (1994-2017), runoff volume increased disproportionately from upstream to downstream stations; for example, although the uppermost subcatchment covered only 22% of the catchment, it contributed 64% of its total mean annual runoff volume (i.e., 3.31 × 10^7 and 5.15 × 10^7 m^3 yr^{-1} at the SILB and HAUS stations, respectively). The spatial contribution of mean annual $NO_3^- - N$ load generally followed that of flow volume (e.g., 68 t yr^{-1} at the SILB station was 43% of the total at the HAUS station). Differences in runoff volume and $NO_3^- - N$ load among subcatchments were due to spatial variability in $NO_3^- - N$ concentrations. From the SILB station to the HAUS station, median $NO_3^- - N$ concentration increased significantly (from 1.01 to 2.68 mg l^{-1}, Wilcoxon signed rank test), while median specific runoff decreased significantly (from 169 to 67 mm yr^{-1}, Wilcoxon signed rank test).

Despite the high spatial variability, discharge and $NO_3^- - N$ concentration showed strong seasonal patterns (Figure 2). Based on the general hydro-climatic cycling (Figure 2a), we categorized the hydrological year into four periods: wetting (October-December, with a continuous increase in mean monthly discharge from 0.90 to 1.80 $m^3 s^{-1}$ at the HAUS station), wet (January-March, with high mean discharge of 2.96 $m^3 s^{-1}$), drying (April-June, with mean monthly discharge decreasing from 2.42 to 0.99 $m^3 s^{-1}$) and dry (July-September, with consistently low mean discharge of 0.58 $m^3 s^{-1}$). The spatial distribution of flow varied greatly among the hydrological periods. The uppermost subcatchment generated most of the catchment's runoff volume during the wet period but much less during the dry period (e.g., mean discharge in February and September was 70% and 53% that at HAUS, respectively) (Figure 2a). The seasonal pattern of $NO_3^- - N$ was similar to that of discharge at the SILB and MEIS stations, with high concentrations (e.g., > 3 mg l^{-1}) during the wet period that gradually decreased during the drying period, and much lower concentrations (e.g., < 1 mg l^{-1}) during the dry period (Figure 2b). However, $NO_3^- - N$ at the HAUS station had consistently high concentrations throughout the hydrological cycle (i.e., generally > 2 mg l^{-1}). Mean $NO_3^- - N$ concentration during the dry period was significantly higher at HAUS (2.60 mg l^{-1}) than at SILB (0.58 mg l^{-1}). The high mean concentrations at HAUS, much higher than those at MEIS and SILB, were likely caused by urban point-source contributions before 2002 (Yang et al., 2018). Nonetheless, the mean monthly concentration decreased slightly from the beginning of the drying period but remained much higher than those at MEIS and SILB.

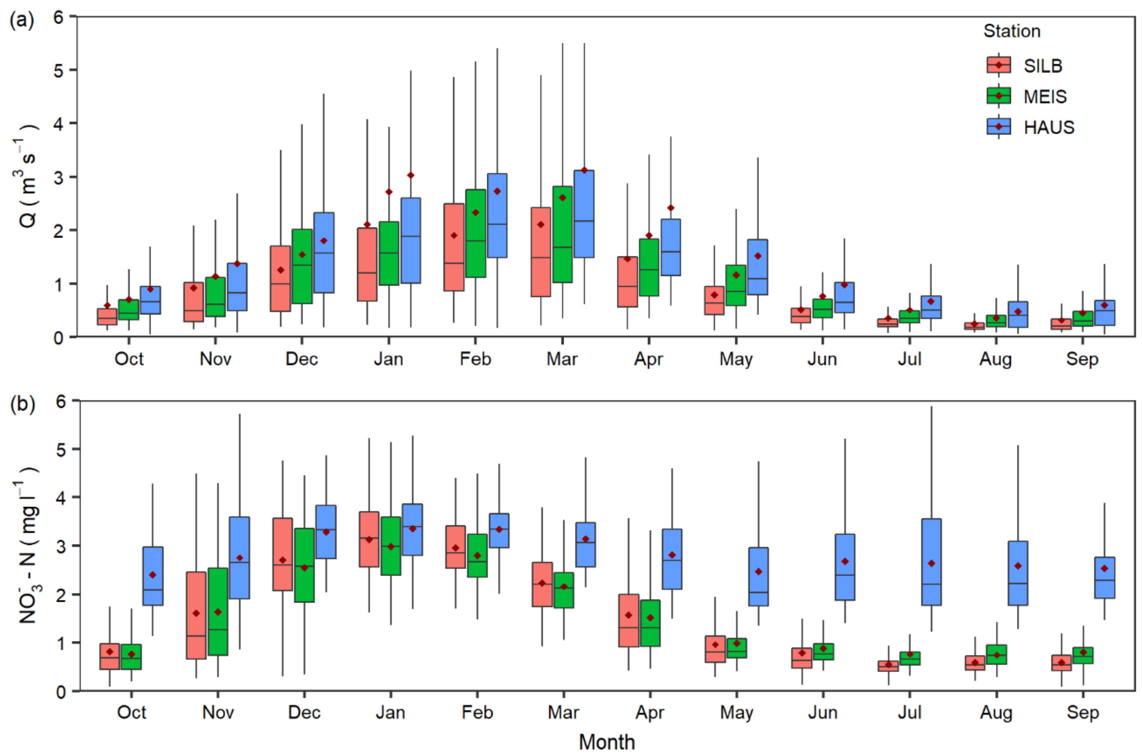

Figure 2. Boxplots of monthly (a) discharge and (b) nitrate-N concentrations at the SILB, MEIS and HAUS stations from 1994-2017. Outliers were omitted, and red diamond markers represent mean values. Whiskers represent 1.5 times the interquartile range.

3.2. Event detection

We analyzed 81, 72, and 70 detected events at the SILB, MEIS and HAUS stations, respectively, from 2012-2017 (Figure 3, Supplementary Table S1). Events were evenly distributed, while their magnitude and duration varied greatly during the four hydrological periods among the three stations (Table 1). Event durations were generally much longer during wetting/wet periods than during drying/dry periods (e.g., mean durations at the SILB station were 11.79 and 4.07 days during the wet and dry periods, respectively). Similarly, event-scale mean discharge and $NO_3^- - N$ had the highest values during the wet period and the lowest values during the dry period at the three stations (Table 1).

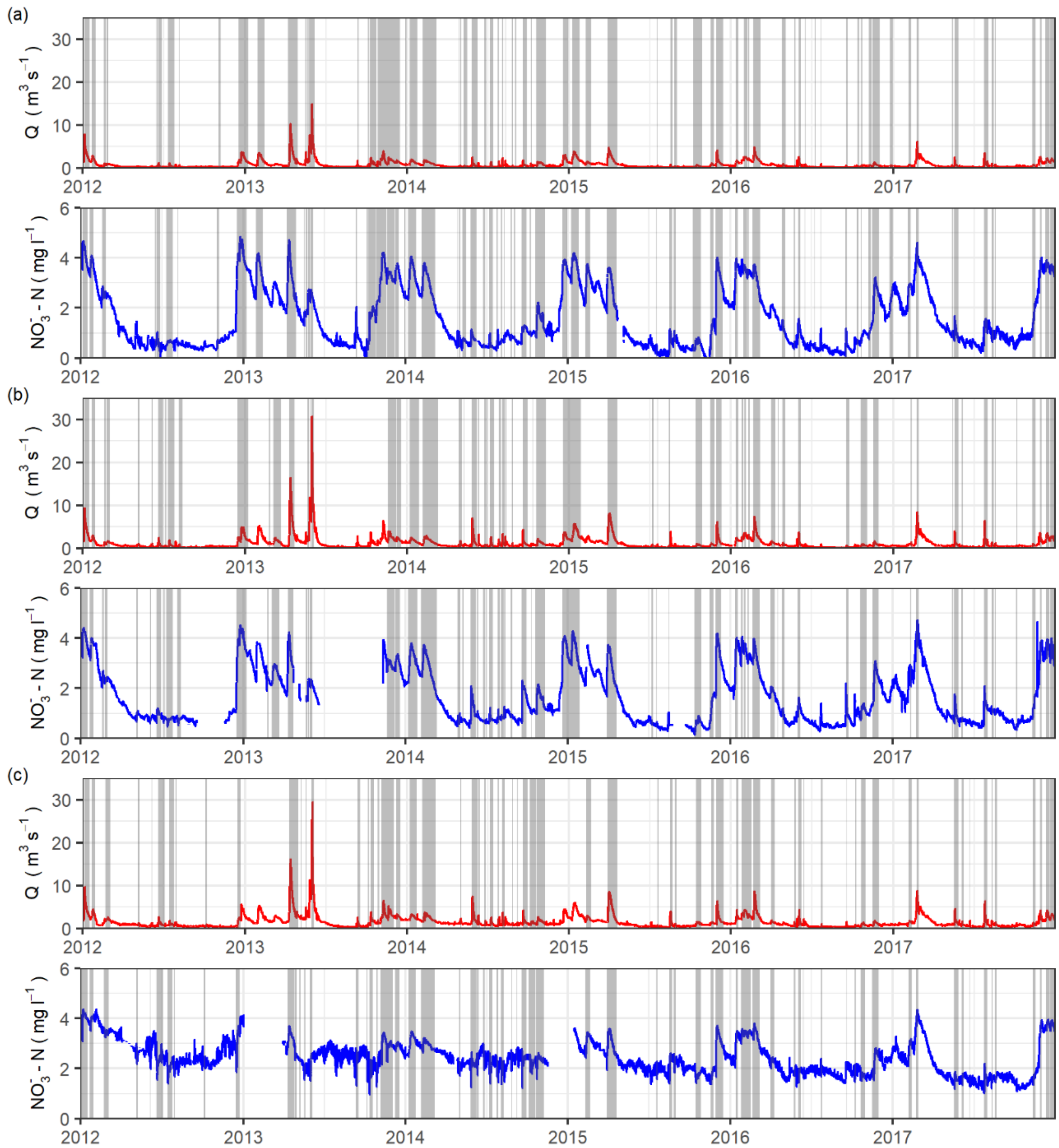

Figure 3. Discharge (Q) and $NO_3^- - N$ concentrations at 15-minute intervals from 2012-2017 at the (a) SILB, (b) MEIS and (c) HAUS stations. A total of 81, 72, and 70 storm events (shaded areas) remained after manual adjustment, respectively.

Table 1. Number of storm events, mean duration, mean discharge (Q) and mean $NO_3^- - N$ concentration during each hydrological period at the SILB, MEIS and HAUS stations.

	SILB				MEIS				HAUS			
Periods	Wetting	Wet	Drying	Dry	Wetting	Wet	Drying	Dry	Wetting	Wet	Drying	Dry
Number	25	16	20	20	17	18	20	17	20	15	18	17
Duration (days)	9.5	11.8	5.1	4.1	11.0	11.0	4.7	5.4	9.2	11.6	5.4	4.8
Q (m^3 s^{-1})	1.12	1.95	1.42	0.56	1.73	2.56	2.42	0.85	1.93	3.29	2.69	1.21
NO_3^--N (mg l^{-1})	2.29	3.38	1.30	0.85	2.42	3.15	1.24	0.98	2.49	3.33	2.16	2.04

3.3. Hysteresis pattern analysis

The patterns of *HI* and *CI* showed both spatial and seasonal variations. Negative *HI* (i.e., counter-clockwise hysteresis) dominated at the SILB, MEIS and HAUS stations (i.e., ca. 78%, 88% and 63% of all events, respectively) (Figure 4a). Most events with positive *HI* (i.e., clockwise hysteresis) occurred during drying/dry periods (78%, 67% and 88% at the SILB, MEIS and HAUS stations, respectively). The median *HI* was significantly different among four hydrological periods at each station (Kruskal-Wallis test). The trend for *CI* differed from that of *HI*. Positive *CI* (i.e., accretion effect) dominated in the uppermost and middle subcatchments (i.e., 89% and 79% of all events at the SILB and MEIS stations, respectively) (Figure 4b). However, 66% of events at the HAUS station had negative *CI* (i.e., dilution effect). The median *CI* between SILB and HAUS, and between MEIS and HAUS were significantly different (Wilcoxon signed rank test). Mean *CI* was positive during all four hydrological periods at the SILB and MEIS stations but was positive only during the wet period at the HAUS station (Figure 4b).

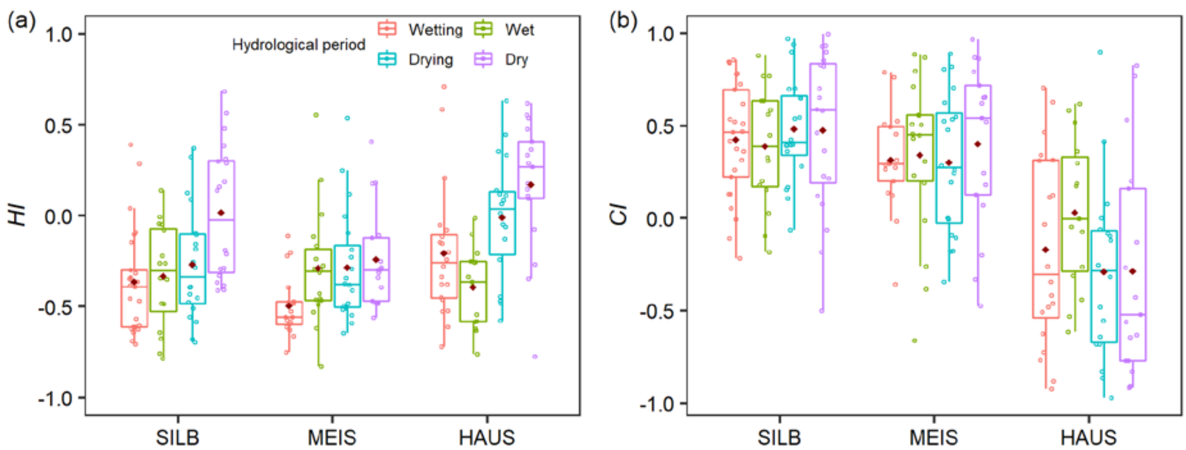

Figure 4. Boxplots of (a) hysteresis index (*HI*) and (b) concentration-change index (*CI*) of storm events during four hydrological periods at the SILB, MEIS and HAUS stations. Red points represent means. Whiskers represent 1.5 times the interquartile range.

We combined the two hysteresis indices and categorized all events into four categories (Figure 5). Event-scale hysteresis patterns varied greatly among the hydrological periods and landscape conditions (Figure 6). At the SILB station, the general hysteresis pattern was negative *HI* combined with positive *CI* (ca. 72%, Figure 6). The events in this category had the longest duration and highest total precipitation (Table 2). The pattern of positive *HI* combined with positive *CI* accounted for 17% of events at SILB, most of which occurred during drying/dry periods. Among events with negative *CI*, those combined with negative *HI* occurred during wetting/wet periods (Figure 6). In contrast, events with positive *HI* occurred during drying/dry periods and had the shortest duration, lowest total precipitation and lowest discharge and $NO_3^- - N$ concentration (Table 2).

At the MEIS station, the general hysteresis pattern was the same as at the SILB station (i.e., 71% of events had negative *HI* with positive *CI*), but the percentage of positive *HI* with positive *CI* decreased to 8%, indicating an overall lower accretion effect (Table 2). Patterns of negative *HI* with negative *CI* increased to 17% of events at MEIS, with a relatively short duration and low discharge (Table 2). The pattern of positive *HI* with negative *CI* was least common and was evenly distributed among the wetting, drying and dry periods (Figure 6). Similarly, this pattern had the shortest duration and lowest total precipitation, discharge and $NO_3^- - N$ concentration (Table 2).

The hysteresis pattern at the HAUS station differed strongly from those at the two upstream stations (Figure 6). The percentage of events with negative *HI* combined with positive *CI*, which dominated at upstream stations, decreased to only 27% at HAUS and had the longest duration, highest total precipitation and highest discharge and $NO_3^- - N$ concentration (Table 2). The general pattern was negative *HI* with negative *CI*, which accounted for ca. 36% of all events. The pattern of positive *HI* with negative *CI* increased from < 5% at the upper two stations to 30% at the HAUS station. The pattern of positive *HI* with positive *CI* occurred only during drying/dry periods (Figure 6). Notably, regardless of *CI*, patterns with positive *HI* usually occurred during drying/dry periods (ca. 88%), with a short duration and low discharge and $NO_3^- - N$ concentration, while patterns with negative *HI* occurred more during wetting/wet periods (ca. 73%), with a long duration and high discharge and $NO_3^- - N$ concentration (Table 2).

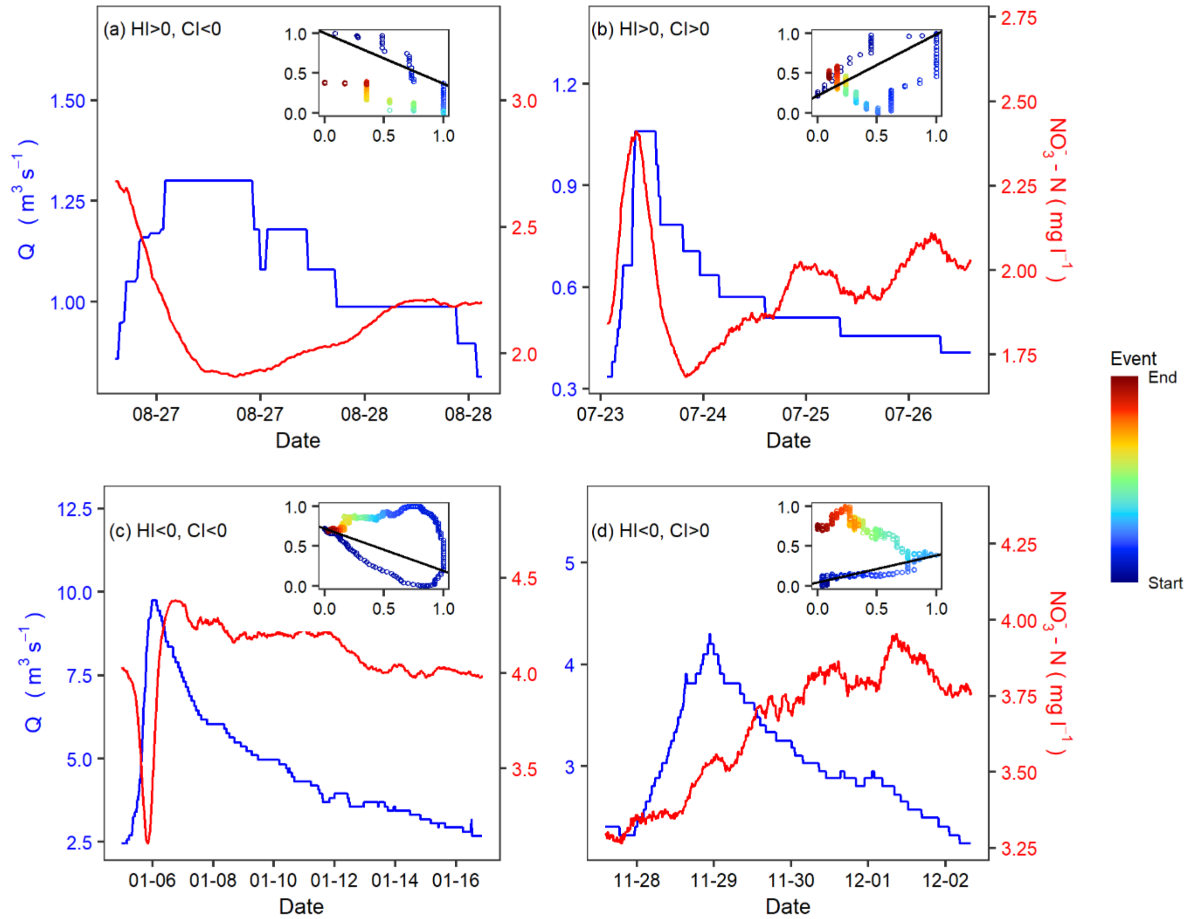

Figure 5. Examples of the four hysteresis types detected at the HAUS station: (a) an event in Aug. 2014 with a positive hysteresis index (*HI*) and positive concentration-change index (*CI*); (b) event in Jul. 2016 with a positive *HI* and negative *CI*; (c) event in Jan. 2012 with a negative *HI* and positive *CI*; and (d) event in Nov. 2017 with a negative *HI* and negative *CI*. Blue and red lines represent discharge and $NO_3^- - N$ concentration, respectively. Inset plots show the corresponding hysteresis loops (from blue to red), in which the x-axis and y-axis are normalized values of discharge and $NO_3^- - N$ concentration, respectively.

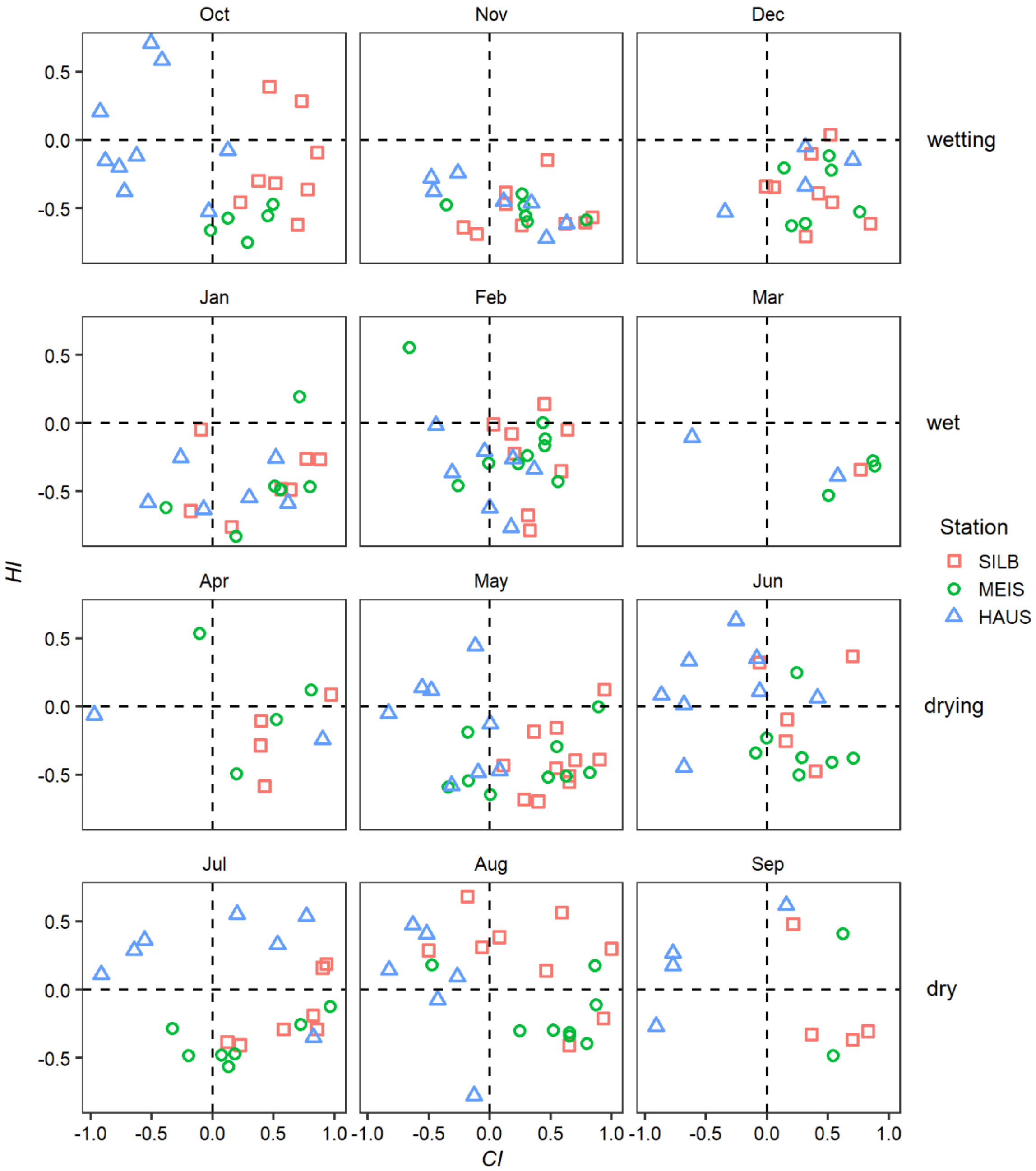

Figure 6. Hysteresis index (*HI*) and concentration-change index (*CI*) patterns at the SILB, MEIS and HAUS stations during the wetting, wet, drying and dry periods.

Table 2. Statistics of events of four hysteresis types based on sign of the hysteresis index (*HI*) and concentration-change index (*CI*) at the SILB, MEIS and HAUS stations (including number of storm events, mean duration, mean total precipitation (P), mean discharge (Q) and mean $NO_3^- - N$ concentration.

	SILB				MEIS				HAUS			
(*HI*/*CI*)	(+/+)	(+/-)	(-/+)	(-/-)	(+/+)	(+/-)	(-/+)	(-/-)	(+/+)	(+/-)	(-/+)	(-/-)
Number	14	4	58	5	6	3	51	12	5	21	19	25
Duration (day)	4.6	2.5	8.7	6.7	14.0	4.4	8.0	5.4	2.1	4.8	10.2	9.3
Total P (mm)	18.70	4.17	27.66	20.00	27.60	7.52	23.78	20.26	12.32	20.45	22.64	19.28
Q ($m^3 s^{-1}$)	0.90	0.63	1.28	1.85	2.60	0.89	1.89	1.62	0.88	1.19	3.66	2.32
NO_3^--N ($mg\ l^{-1}$)	1.23	0.78	2.05	3.01	2.07	1.52	1.92	1.74	1.99	2.11	2.99	2.49

3.4. Shared events analysis

To investigate the influence of the landscape on seasonal flow and nitrate dynamics, we analyzed 24 catchment-wide shared events. Most shared events had negative *HI* at the SILB and MEIS stations, with only one event with positive *HI* at the MEIS station (Supplementary Table S2). Three shared events had positive *HI* during the dry period at the HAUS station, with a high contribution of $NO_3^- - N$ load from the lowermost subcatchment (Table S2). The number of shared events with negative *CI* increased from upstream to downstream (i.e., 2, 3 and 12 at the SILB, MEIS and HAUS stations, respectively) (Table S2).

Runoff volume (R_V) and nitrate-N load (N_L) contributions from each subcatchment had strong seasonal variations at the event scale (Figure 7). During wetting/wet periods, $R_{V,UP}$: $R_{V,ALL}$ was significantly higher than $R_{V,MID}$: $R_{V,ALL}$ and $R_{V,LOW}$: $R_{V,ALL}$ (Kruskal-Wallis test). $R_{V,MID}$: $R_{V,ALL}$ and $R_{V,LOW}$: $R_{V,ALL}$ varied during the wetting period, but the former ratio increased and the latter one decreased during the wet period. During the drying period, $R_{V,UP}$: $R_{V,ALL}$ decreased quickly to a proportion similar to $R_{V,MID}$: $R_{V,ALL}$, while $R_{V,LOW}$: $R_{V,ALL}$ increased but remained lower than $R_{V,UP}$: $R_{V,ALL}$ and $R_{V,MID}$: $R_{V,ALL}$. During the dry period, contributions from the three subcatchments varied within a similar range, with slightly higher $R_{V,UP}$: $R_{V,ALL}$ than $R_{V,MID}$: $R_{V,ALL}$ and $R_{V,LOW}$: $R_{V,ALL}$.

Nitrate-N load contributions had a different seasonal pattern from runoff volume contributions (Figure 7b). During wetting/wet periods, nitrate-N load contributions from the three subcatchments generally followed runoff volume contributions (i.e., that from the uppermost subcatchment was significantly higher than that form the middle and lowermost subcatchments, Kruskal-Wallis test). Likewise, $N_{L,MID}$: $N_{L,ALL}$ and $N_{L,LOW}$: $N_{L,ALL}$ varied, with the former ratio increasing and the latter one decreasing. During the drying period, however, $N_{L,MID}: N_{L,ALL}$ increased quickly and ultimately exceeded $N_{L,UP}: N_{L,ALL}$, while both $N_{L,UP}: N_{L,ALL}$ and $N_{L,MID}: N_{L,ALL}$ decreased to a similar low proportion. During the dry period, $N_{L,LOW}: N_{L,ALL}$ decreased. Thus, the subcatchment that contributed the most nitrate-N load varied among the four hydrological periods.

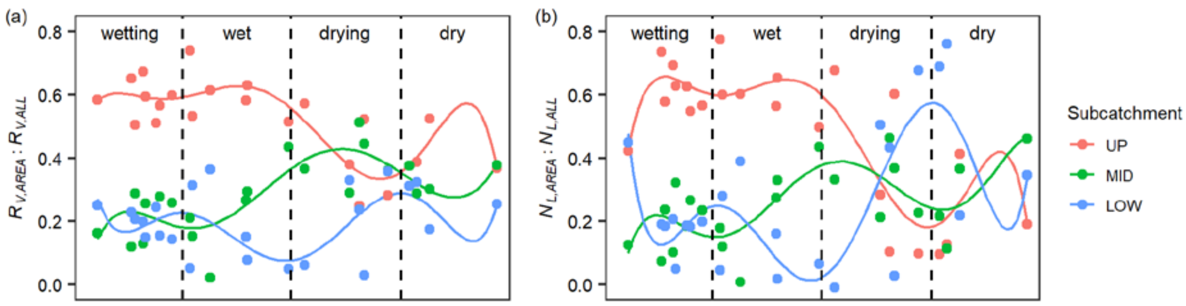

Figure 7. Contribution of (a) runoff volume (R_V) and (b) nitrate-N load (N_L) from each subcatchment to the catchment outlet for shared events throughout the year. Dashed lines separate the four hydrological periods. Solid lines indicate high-order polynomial regressions.

4. Discussion

Terrestrial nitrate transport at the catchment scale is strongly related to flow dynamics. In the Selke catchment, the land-to-stream transport has been identified as a key driven factor for surface water dynamics (Dupas et al., 2017). Due to the complex combination of meteorological, hydrological, geographical and pedological characteristics of each subcatchment, nitrate dynamics varied from upstream to downstream in the nested Selke catchment. Based on the hysteresis indices, four hysteresis patterns can be conceptualized (Figure 8). The driving factors of their occurrences in the Selke catchment (Figure 6) depend on the combinations of landscape features and hydrological conditions at the seasonal scale.

4.1. Characteristic patterns of flow and nitrate dynamics

The four hysteresis patterns varied strongly spatially and temporally. In the uppermost and forest-dominated middle subcatchments, the most common hysteresis pattern across different seasons was counter-clockwise hysteresis with an accretion effect during the rising limb (i.e., negative *HI* with positive *CI*, c.a. 70% at the SILB and MEIS stations). At the event scale, nitrate sources near stream reaches were flushed out quickly, which resulted in an accretion effect during the rising limb of the hydrograph, given the low ambient nitrate concentrations (Figure 8d). Although the uppermost mountainous regions contain considerable areas of agricultural land, nitrate cannot accumulate in the deeper subsurface due to the shallow impermeable bedrock and the consequently flashier flow pathways (Dupas et al., 2017; Yang et al., 2019). This feature results in higher nitrate concentrations in the interflow than in the baseflow. Consequently, a synchronous seasonal pattern of discharge and nitrate concentration was observed (i.e., generally high values during wetting/wet interflow-dominated periods and low values during drying/dry baseflow-dominated periods, Figure 2). Due to sufficient precipitation during events and well-established hydrological connectivity, interflow can transport distal terrestrial nitrate sources to the stream, which further increases surface water nitrate concentrations. The time lag between hydrological celerity and solute transport velocity makes nitrate concentration normally peak after discharge do, which results in counter-clockwise hysteresis. However, this pattern decreased at the HAUS station, accounting for only 27 % and occurred more frequently during wetting/wet periods. Under high-flow and low-temperature conditions, the pattern at the catchment outlet was controlled more by the two upstream subcatchments due to their large contributions to both runoff volume and nitrate-N load (Figure 7) and low in-stream nitrate uptake (Rode et al., 2016a). Therefore, during wetting/wet periods, the hysteresis pattern at the HAUS station can depend more on upstream features than on those of the lowermost subcatchment.

The propagation effects also influenced the pattern of counter-clockwise hysteresis with a dilution effect at the three stations (Figure 8c). The uppermost and middle subcatchments had more saturation overland flow with lower nitrate concentration in forest areas (Zimmermann et al., 2006). Overland flow near streams can be generated quickly during wetting/wet periods with high discharge, causing a dilution effect at the beginning of events. The dominant runoff component of overland flow during the rising limb can be replaced by interflow quickly, with higher nitrate concentration, resulting in counter-clockwise hysteresis. This pattern was the most common pattern at the HAUS station. During wetting/wet periods, this hysteresis pattern at HAUS can be affected by the two upstream subcatchments as mentioned. Moreover, stream water routed from upstream subcatchments can also dilute nitrate concentration in the lowermost subcatchment, since the latter generally has higher nitrate concentration during low flow conditions (Figure 2), changing the hysteresis pattern from upstream accretion to downstream dilution across different seasons (Table S2). Besides influences from upstream subcatchments, features of the lowermost subcatchment can also cause a dilution effect. Urban/arable areas have been recognized to influence runoff generation in a catchment during storm events (Bronstert et al., 2002; Niehoff et al., 2002). Agricultural and municipal construction results in quick surface flow, which tends to decrease nitrate concentration. Dilution effects caused by surface flow during storm events were also observed in a mountainous agricultural catchment in California (USA) (Goodridge and Melack, 2012), mountainous agricultural catchments in the tropics (Jacobs et al., 2018) and urbanized catchments in North America (Barco et al., 2008). In this case, nitrate concentration decreased quickly at the beginning of the rising limb in the uppermost and lowermost subcatchments (Figure 5c), which both contain urban and arable areas (Figure 1). Interflow can then dominate quickly due to hydrological connectivity during wet periods, or baseflow can dominate again after quick flow during the dry period. In both situations, nitrate concentration increased after quick flow before the discharge peak, resulting in counter-clockwise hysteresis (Figure 8c). Therefore, this pattern dominated at the HAUS station not only due to events that propagated from upstream subcatchments, but also events generated in the lowermost subcatchment.

It was noticeable that clockwise hysteresis occurred more during drying/dry periods (Figure 6). Hydrological connectivity from land to stream can be limited by the higher temperature and lower soil moisture during drying/dry periods. Distal nitrate sources become immobilized and are not exported to the stream at low discharge, and thus resulted in clockwise hysteresis (Figure 5a). Our findings are in line with those of Baker and Showers (2019) who concluded that clockwise hysteresis was favored when antecedent soil moisture was low. In the uppermost subcatchment, the accretion effect was caused by plentiful proximal nitrate sources, as mentioned. In the middle subcatchment, atmospheric deposition is the main source of N in forest areas (MacDonald et al., 2002). Nitrate concentration has been reported to be higher in the topsoil than in groundwater due to uptake by deep-rooted vegetation and denitrification in deep soil layers (Chaves et al., 2009). Consequently, fewer distal nitrate sources can be transported to the stream during the baseflow-dominated dry period in the middle than in the uppermost subcatchment, which decreased the number of clockwise hysteresis at the MEIS station (Table 2). This pattern was the least common pattern at the HAUS station and occurred only during drying/dry periods (Figure 6). None of this pattern at HAUS belonged to shared event (Table S2). This indicated that this pattern could represent nitrate dynamics exclusively in the lowermost subcatchment. The lowermost subcatchment usually stores more nitrate due to mineral fertilizer and manure application. Saturated nitrate sources that are near the stream are easily flushed out when storm events occur, even at low discharge, leading to accretion effects (Figure 8b). Subsequently, nitrate concentration decreases quickly due to insufficient precipitation and low hydrological connectivity with distal nitrate sources, resulting in clockwise hysteresis.

The features of the lowermost subcatchment caused more clockwise hysteresis with the dilution effect (Figure 8a), which was the second-most common pattern at the HAUS station. This pattern appeared more during drying/dry periods when the lowermost subcatchment contributed considerable nitrate-N load and had substantial influence on nitrate export dynamics (Figure 7b). In this situation, the dilution effect at the HAUS station could be related to quick flow from paved areas in the lowermost subcatchment, as mentioned. Nitrate concentration followed a vertical gradient in the lowermost subcatchment: lower in the topsoil due to plant uptake and higher in deep soil due to legacy nitrate (Outram et al., 2016). Hydrological connectivity was low during drying/dry periods, and interflow could not increase enough to transport deep nitrate-rich sources to the stream, which results in the continued decrease in nitrate concentration during the falling limb. Therefore, clockwise hysteresis occurred more at the HAUS station than at the two upstream stations (i.e., only 4 and 3 times at SILB and MEIS, respectively).

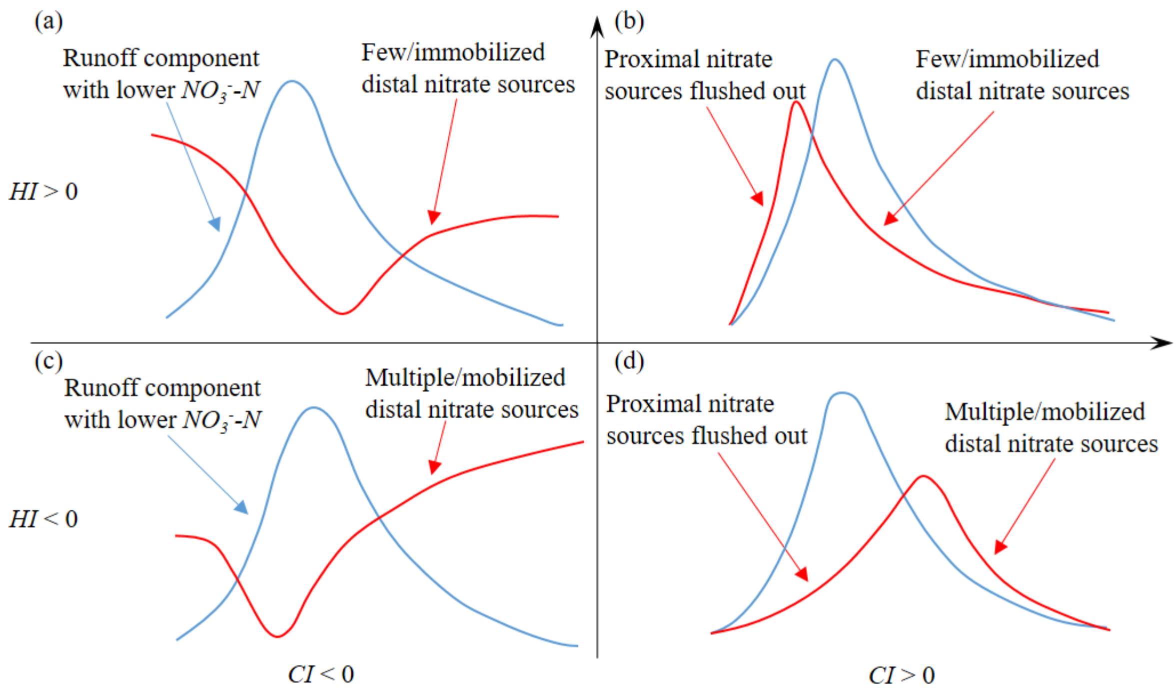

Figure 8. Conceptual interpretation of nitrate-discharge relationships during events for the four combinations of hysteresis index (*HI*) and concentration-change index (*CI*). Blue lines indicate flow behavior, and red lines indicate $NO_3^- - N$ behavior. Arrows indicate dominant mechanisms during rising/falling limbs.

4.2. Implications and limits

Overall, the hysteresis pattern based on the C-Q relationship varied among landscapes, reflecting unique flow pathways and spatial nitrate storage. Due to different human activities (e.g., fertilizer application, drainage construction) and geological conditions, different patterns can dominate for a given dominant land use. For example, Carey et al. (2014) observed more clockwise hysteresis and a dilution effect in coastal catchments in which forest dominated. In contrast, we observed that counter-clockwise hysteresis with an accretion effect dominated in the upstream mountainous forest areas. This difference indicates that scientific monitoring should be set up according to meteorological, hydrological, geographical and pedological features rather than based only on land use. This is especially important in a nested catchment, where upstream subcatchment(s) can influence downstream subcatchment(s), and thus conceal nutrient export dynamics of the latter. Furthermore, differences in hydrological connectivity and biogeochemical processes due to seasonal variations can cause variable flow and nitrate dynamics (e.g., more clockwise hysteresis during drying/dry periods and more counter-clockwise hysteresis during wetting/wet periods). To disentangle seasonal effects, long-term high-frequency monitoring can provide reliable datasets. Our findings can be used to target mitigation measures when specific *HI*/*CI* combinations dominate in a given catchment. For example, when the C-Q relationship suggests that proximal nitrate sources dominate, management actions can focus on agricultural land near streams, but when distal nitrate sources dominate, catchment-wide actions are required.

However, hysteresis analysis should also consider hydrographs with dual peaks or extremely long recession periods, which may influence the analysis (Lloyd et al., 2016b; Williams et al., 2018). Such hydrographs were rare in our study, but since they can improve understanding of process mechanisms during certain periods, they were not excluded. For example, the only shared event with positive *HI* at the MEIS station showed counter-clockwise hysteresis early in the event but was influenced by a dual peak and longer falling limb, which yielded a low positive value of *HI* (ca. 0.006). This analysis can improve understanding of the corresponding shared event at the SILB station that had negative *HI*: multiple distal sources can be consumed after a long period of flushing (e.g., during a large storm event) and cause lower nitrate concentrations during the late falling limb. This case requires catchment-wide management actions instead of focus on proximal streams, despite a positive *HI* at the MEIS station. Thus, events should be assessed carefully to avoid unreliable conclusions from statistical results, especially those with low values of *HI* or *CI*. Doing so may provide a detailed picture of variations in flow/nitrate dynamics.

Our comprehensive analysis of landscape and seasonality effects on flow and nitrate dynamics focused mainly on high-frequency monitoring data. Therefore, it is difficult to quantify the landscape effect in the three subcatchments of the Selke catchment, even when considering shared events. The landscape effect should be explored further using physical-based hydrological water-quality models. Current modeling is based mainly on daily data (Yang et al., 2018), which may bias detection of storm events and calculation of the nitrate-N load during storm events. Thus, future studies require high-frequency modeling, which can be used to quantify influential factors that result in different flow and nitrate dynamics and provide targeted advice for water management.

5. Conclusions

According to C-Q relationships, counter-clockwise hysteresis with an accretion effect dominated the catchment throughout the year; however, hysteresis was clockwise during specific periods in each subcatchment. Clockwise hysteresis occurred more during the dry period, indicating low hydrological connectivity from land to stream for export of distal nitrate sources. Dilution effects dominated in the lowermost catchment, which may have been influenced by flow propagating from upstream subcatchments during the wet period or generated by quick flow from paved areas.

When analyzing shared events, the uppermost subcatchment always dominated runoff volume and dominated nitrate-N load during all periods except the dry period, when the lowermost subcatchment dominated nitrate-N load, which indicates the substantial contribution of nitrate export regimes from the lower urban/arable area. At the event scale, this alternation suggests that high nitrate-loaded interflow dominated in the upper mountainous subcatchments, while quick runoff (e.g., surface flow with low nitrate concentration) dominated in the lowermost subcatchment. This difference in nitrate export can increase during dry/hot seasons, when hydrological connectivity and biogeochemical processes change greatly.

These conclusions depend greatly on high-frequency data, which enabled events to be detected and nitrate-N load to be calculated more accurately. Although complex hydrographs may have influenced our results, the interpretation of the fundamental mechanism of variable C-Q relationships remains reliable. Water or agricultural management should be considered in complex conditions in which several mechanisms may coexist. Thus, a continuous and scientific monitoring strategy in a nested catchment is important to capture the nitrate export regime at the seasonal and catchment scale.

Acknowledgement

Xiaolin Zhang is funded by Chinese Scholarship Council (CSC). We would like to thank the Editor Huaming Guo, the Associate Editor Rafael Perez Lopez and the two anonymous Reviewers for their thoughtful comments. The high-frequency nitrate data are provided by TERENO (Terrestrial

Environment Observatories) project. We thank the State Agency for Flood Protection and Water Management of Saxony-Anhalt (LHW) for providing high-frequency discharge data, German Weather Service (DWD) for providing precipitation data.

References

Allen, A.P., Brown, J.H., Gillooly, J.F., 2002. Global biodiversity, biochemical kinetics, and the energetic-equivalence rule. Science. 297, 1545–1548. https://doi.org/10.1126/science.1072380.

Baker, E.B., Showers, W.J., 2019. Hysteresis analysis of nitrate dynamics in the Neuse River, NC. Sci. Total Environ. 652, 889–899. https://doi.org/10.1016/j.scitotenv.2018.10.254.

Barco, J., Hogue, T.S., Curto, V., Rademacher, L., 2008. Linking hydrology and stream geochemistry in urban fringe watersheds. J. Hydrol. 360, 31–47. https://doi.org/10.1016/j.jhydrol.2008.07.011.

Borken, W., Matzner, E., 2004. Nitrate leaching in forest soils: an analysis of long-term monitoring sites in Germany. J. Plant Nutr. Soil Sci. 167, 277–283. https://doi.org/10.1002/jpln.200421354.

Bowes, M.J., Jarvie, H.P., Halliday, S.J., Skeffington, R.A., Wade, A.J., Loewenthal, M., Gozzard, E., Newman, J.R., Palmer-Felgate, E.J., 2015. Characterising phosphorus and nitrate inputs to a rural river using high-frequency concentration–flow relationships. Sci. Total Environ. 511, 608–620. https://doi.org/10.1016/j.scitotenv.2014.12.086.

Boyer, E.W., Goodale, C.L., Jaworski, N.A., Howarth, R.W., 2002. Anthropogenic nitrogen sources and relationships to riverine nitrogen export in the northeastern U.S.A. Biogeochemistry 57, 137–169. https://doi.org/10.1023/A:1015709302073.

Bracken, L.J., Croke, J., 2007. The concept of hydrological connectivity and its contribution to understanding runoff-dominated geomorphic systems. Hydrol. Process. 21, 1749–1763. https://doi.org/10.1002/hyp.6313.

Bronstert, A., Niehoff, D., Bürger, G., 2002. Effects of climate and land-use change on storm runoff generation: present knowledge and modelling capabilities. Hydrol. Process. 16, 509–529. https://doi.org/10.1002/hyp.326.

Burns, D.A., Pellerin, B.A., Miller, M.P., Capel, P.D., Tesoriero, A.J., Duncan, J.M., 2019. Monitoring the riverine pulse: Applying high-frequency nitrate data to advance integrative understanding of biogeochemical and hydrological processes. Wiley Interdiscip. Rev. Water e1348. https://doi.org/10.1002/wat2.1348.

Butturini, A., Alvarez, M., Bernal, S., Vazquez, E., Sabater, F., 2008. Diversity and temporal sequences of forms of DOC and NO_3-discharge responses in an intermittent stream: Predictable or random succession? J. Geophys. Res. 113. https://doi.org/10.1029/2008jg000721.

Carey, R.O., Wollheim, W.M., Mulukutla, G.K., Mineau, M.M., 2014. Characterizing storm-event nitrate fluxes in a fifth order suburbanizing watershed using in situ sensors. Env. Sci Technol. 48, 7756–7765. https://doi.org/10.1021/es500252j.

Chaves, J., Neill, C., Germer, S., Gouveia Neto, S., Krusche, A. V, Castellanos Bonilla, A., Elsenbeer, H., 2009. Nitrogen Transformations in Flowpaths Leading from Soils to Streams in Amazon Forest and Pasture. Ecosystems 12, 961–972. https://doi.org/10.1007/s10021-009-9270-4.

Cheraghi, M., Jomaa, S., Sander, G.C., Barry, D.A., 2016. Hysteretic sediment fluxes in rainfall-driven soil erosion: Particle size effects. Water Resour. Res. 52, 8613–8629. https://doi.org/10.1002/2016wr019314.

Davidson, E.A., David, M.B., Galloway, J.N., Goodale, C.L., Haeuber, R., Harrison, J.A., Howarth, R.W., Jaynes, D.B., Lowrance, R.R., Thomas Nolan, B., Peel, J.L., Pinder, R.W., Porter, E., Snyder, C.S., Townsend, A.R., Ward, M.H., 2011. Excess nitrogen in the U.S. environment: Trends, risks, and solutions. Issues Ecol. (available at https://pubs.er.usgs.gov/publication/70032270, last accessed on 9.6.2020)

Dupas, R., Jomaa, S., Musolff, A., Borchardt, D., Rode, M., 2016. Disentangling the influence of hydroclimatic patterns and agricultural management on river nitrate dynamics from sub-hourly to decadal time scales. Sci. Total Environ. 571, 791–800. https://doi.org/10.1016/j.scitotenv.2016.07.053.

Dupas, R., Musolff, A., Jawitz, J.W., Rao, P.S.C., Jäger, C.G., Fleckenstein, J.H., Rode, M., Borchardt, D., 2017. Carbon and nutrient export regimes from headwater catchments to downstream reaches. Biogeosciences 14, 4391–4407. https://doi.org/10.5194/bg-14-4391-2017.

EEA, 2018. European waters -- Assessment of status and pressures 2018. European Environmenta Agency, Copenhagen, Denmark.

EEA, 2019. Nutrients in freshwater in Europe. European Environment Agency, Copenhagen, Denmark.

Fovet, O., Humbert, G., Dupas, R., Gascuel-Odoux, C., Gruau, G., Jaffrezic, A.,Thelusma, G., Faucheux, M., Gilliet, N., Hamon, Y., Grimaldi, C., 2018. Seasonal variability of stream water quality response to storm events captured using high-frequency and multi-parameter data. J. Hydrol. 559, 282–293. https://doi.org/10.1016/j.jhydrol.2018.02.040

Goodridge, B.M., Melack, J.M., 2012. Land use control of stream nitrate concentrations in mountainous coastal California watersheds. J. Geophys. Res. Biogeosciences 117, G02005. https://doi.org/10.1029/2011JG001833.

Howarth, R., Swaney, D., Billen, G., Garnier, J., Hong, B., Humborg, C., Johnes, P., Mörth, C.-M., Marino, R., 2012. Nitrogen fluxes from the landscape are controlled by net anthropogenic nitrogen inputs and by climate. Front. Ecol. Environ. 10, 37–43. https://doi.org/10.1890/100178.

Jacobs, S.R., Weeser, B., Guzha, A.C., Rufino, M.C., Butterbach-Bahl, K., Windhorst, D., Breuer, L., 2018. Using High-Resolution Data to Assess Land Use Impact on Nitrate Dynamics in East African Tropical Montane Catchments. Water Resour. Res. 54, 1812–1830. https://doi.org/10.1002/2017wr021592.

Jiang, S.Y., Zhang, Q., Werner, A.D., Wellen, C., Jomaa, S., Zhu, Q.D., Büttner, O., Meon, G., Rode, M., 2019. Effects of stream nitrate data frequency on watershed model performance and prediction uncertainty. J. Hydrol. 569, 22–36. https://doi.org/10.1016/j.jhydrol.2018.11.049.

Kruskal, W.H., Wallis, W.A., 1952. Use of Ranks in One-Criterion Variance Analysis. J. Am. Stat. Assoc. 47, 583–621. https://doi.org/10.1080/01621459.1952.10483441.

Lloyd, C.E.M., Freer, J.E., Johnes, P.J., Collins, A.L., 2016a. Technical Note: Testing an improved index for analysing storm discharge-concentration hysteresis. Hydrol. Earth Syst. Sci. 20, 625–632. https://doi.org/10.5194/hess-20-625-2016.

Lloyd, C.E.M., Freer, J.E., Johnes, P.J., Collins, A.L., 2016b. Using hysteresis analysis of high-resolution water quality monitoring data, including uncertainty, to infer controls on nutrient and sediment transfer in catchments. Sci. Total Environ. 543, 388–404. https://doi.org/10.1016/j.scitotenv.2015.11.028.

MacDonald, J.A., Dise, N.B., Matzner, E., Armbruster, M., Gundersen, P., Forsius, M., 2002. Nitrogen input together with ecosystem nitrogen enrichment predict nitrate leaching from European forests. Glob. Chang. Biol. 8, 1028–1033. https://doi.org/10.1046/j.1365-2486.2002.00532.x.

McDonnell, J.J., Beven, K., 2014. Debates—The future of hydrological sciences: A (common) path forward? A call to action aimed at understanding velocities, celerities and residence time distributions of the headwater hydrograph. Water Resour. Res. 50, 5342–5350. https://doi.org/10.1002/2013WR015141.

Miller, J.D., Kim, H., Kjeldsen, T.R., Packman, J., Grebby, S., Dearden, R., 2014. Assessing the impact of urbanization on storm runoff in a peri-urban catchment using historical change in impervious cover. J. Hydrol. 515, 59–70. https://doi.org/10.1016/j.jhydrol.2014.04.011.

Miller, M.P., Tesoriero, A.J., Hood, K., Terziotti, S., Wolock, D.M., 2017. Estimating Discharge and Nonpoint Source Nitrate Loading to Streams From Three End-Member Pathways Using High-Frequency Water Quality Data. Water Resour. Res. 53, 10201–10216. https://doi.org/10.1002/2017wr021654.

Molenat, J., Gascuel-Odoux, C., Ruiz, L., Gruau, G., 2008. Role of water table dynamics on stream nitrate export and concentration in agricultural headwater catchment (France). J. Hydrol. 348, 363–378. https://doi.org/10.1016/j.jhydrol.2007.10.005.

Musolff, A., Schmidt, C., Selle, B., Fleckenstein, J.H., 2015. Catchment controls on solute export. Adv. Water Resour. 86, 133–146. https://doi.org/10.1016/j.advwatres.2015.09.026.

Musolff, A., Schmidt, C., Rode, M., Lischeid, G., Weise, S.M., Fleckenstein, J.H., 2016. Groundwater head controls nitrate export from an agricultural lowland catchment. Adv. Water Resour. 96, 95–107. https://doi.org/10.1016/j.advwatres.2016.07.003.

Niehoff, D., Fritsch, U., Bronstert, A., 2002. Land-use impacts on storm-runoff generation: scenarios of land-use change and simulation of hydrological response in a meso-scale catchment in SW-Germany. J. Hydrol. 267, 80–93. https://doi.org/10.1016/S0022-1694(02)00142-7.

Outram, F.N., Cooper, R.J., Sünnenberg, G., Hiscock, K.M., Lovett, A.A., 2016. Antecedent conditions, hydrological connectivity and anthropogenic inputs: Factors affecting nitrate and phosphorus transfers to agricultural headwater streams. Sci. Total Environ. 545–546, 184–199. https://doi.org/10.1016/j.scitotenv.2015.12.025.

Poor, C.J., McDonnell, J.J., 2007. The effects of land use on stream nitrate dynamics. J. Hydrol. 332, 54–68. https://doi.org/10.1016/j.jhydrol.2006.06.022.

R Core Team, 2020. R: A language and environment for statistical computing. R Foundation for Statistical Computing, Vienna, Austria. https://www.R-project.org/.

Racchetti, E., Bartoli, M., Soana, E., Longhi, D., Christian, R.R., Pinardi, M., Viaroli, P., 2011. Influence of hydrological connectivity of riverine wetlands on nitrogen removal via denitrification. Biogeochemistry 103, 335–354. https://doi.org/10.1007/s10533-010-9477-7.

Reusch, T.B.H., Dierking, J., Andersson, H.C., Bonsdorff, E., Carstensen, J., Casini, M., Czajkowski, M., Hasler, B., Hinsby, K., Hyytiäinen, K., Johannesson, K., Jomaa, S., Jormalainen, V., Kuosa, H., Kurland, S., Laikre, L., MacKenzie, B.R., Margonski, P., Melzner, F., Oesterwind, D., Ojaveer, H., Refsgaard, J.C., Sandström, A., Schwarz, G., Tonderski, K., Winder, M., Zandersen, M., 2018. The Baltic Sea as a time machine for the future coastal ocean. Sci. Adv. 4, eaar8195. https://doi.org/10.1126/sciadv.aar8195.

Rode, M., Halbedel Nee Angelstein, S., Anis, M.R., Borchardt, D., Weitere, M., 2016a. Continuous In-Stream Assimilatory Nitrate Uptake from High-Frequency Sensor Measurements. Env. Sci Technol 50, 5685–5694. https://doi.org/10.1021/acs.est.6b00943.

Rode, M., Wade, A.J., Cohen, M.J., Hensley, R.T., Bowes, M.J., Kirchner, J.W., Arhonditsis, G.B., Jordan, P., Kronvang, B., Halliday, S.J., Skeffington, R.A., Rozemeijer, J.C., Aubert, A.H., Rinke, K., Jomaa, S., 2016b. Sensors in the Stream: The High-Frequency Wave of the Present. Env. Sci Technol. 50, 10297–10307. https://doi.org/10.1021/acs.est.6b02155.

Shields, C.A., Band, L.E., Law, N., Groffman, P.M., Kaushal, S.S., Savvas, K., Fisher, G.T., Belt, K.T., 2008. Streamflow distribution of non-point source nitrogen export from urban-rural catchments in the Chesapeake Bay watershed. Water Resour. Res. 44, W09416. https://doi.org/10.1029/2007wr006360.

Sickman, J.O., Leydecker, A., Chang, C.C.Y., Kendall, C., Melack, J.M., Lucero, D.M., Schimel, J., 2003. Mechanisms underlying export of N from high-elevation catchments during seasonal transitions. Biogeochemistry 64, 1–24. https://doi.org/10.1023/A:1024928317057.

Strohmenger, L., Fovet, O., Akkal‐Corfini, N., Dupas, R., Durand, P., Faucheux, M., Gruau, G., Hamon, Y., Jaffrezic, A., Minaudo, C., Petitjean, P., Gascuel‐Odoux, C., 2020. Multi‐temporal relationships between the hydro‐climate and exports of carbon, nitrogen and phosphorus in a small agricultural watershed. Water Resour. Res. https://doi.org/10.1029/2019wr026323.

Vaughan, M.C.H., Bowden, W.B., Shanley, J.B., Vermilyea, A., Sleeper, R., Gold, A.J., Pradhanang, S.M., Inamdar, S.P., Levia, D.F., Andres, A.S., Birgand, F., Schroth, A.W., 2017. High-frequency dissolved organic carbon and nitrate measurements reveal differences in storm hysteresis and loading in relation to land cover and seasonality. Water Resour. Res. 53, 5345–5363. https://doi.org/10.1002/2017wr020491.

Wilcoxon, F., 1945. Individual Comparisons by Ranking Methods. Biometrics Bull. 1, 80–83. https://doi.org/10.2307/3001968.

Williams, M.R., Livingston, S.J., Penn, C.J., Smith, D.R., King, K.W., Huang, C., 2018. Controls of event-based nutrient transport within nested headwater agricultural watersheds of the western Lake Erie basin. J. Hydrol. 559, 749–761. https://doi.org/10.1016/j.jhydrol.2018.02.079.

Wollschläger, U., Attinger, S., Borchardt, D., Brauns, M., Cuntz, M., Dietrich, P., Fleckenstein, J.H., Friese, K., Friesen, J., Harpke, A., Hildebrandt, A., Jäckel, G., Kamjunke, N., Knöller, K., Kögler, S., Kolditz, O., Krieg, R., Kumar, R., Lausch, A., Liess, M., Marx, A., Merz, R., Mueller, C., Musolff, A., Norf, H., Oswald, S.E., Rebmann, C., Reinstorf, F., Rode, M., Rink, K., Rinke, K., Samaniego, L., Vieweg, M., Vogel, H.-J., Weitere, M., Werban, U., Zink, M., Zacharias, S., 2016. The Bode hydrological observatory: a platform for integrated, interdisciplinary hydro-ecological research within the TERENO Harz/Central German Lowland Observatory. Environ. Earth Sci. 76, 29. https://doi.org/10.1007/s12665-016-6327-5.

Yang, X., Jomaa, S., Rode, M., 2019. Sensitivity Analysis of Fully Distributed Parameterization Reveals Insights Into Heterogeneous Catchment Responses for Water Quality Modeling. Water Resour. Res. 55, 10935–10953. https://doi.org/10.1029/2019wr025575.

Yang, X., Jomaa, S., Zink, M., Fleckenstein, J.H., Borchardt, D., Rode, M., 2018. A New Fully Distributed Model of Nitrate Transport and Removal at Catchment Scale. Water Resour. Res. 54, 5856–5877. https://doi.org/10.1029/2017wr022380.

Zacharias, S., Bogena, H., Samaniego, L., Mauder, M., Fuß, R., Pütz, T., Frenzel, M., Schwank, M., Baessler, C., Butterbach-Bahl, K., Bens, O., Borg, E., Brauer, A., Dietrich, P., Hajnsek, I., Helle, G., Kiese, R., Kunstmann, H., Klotz, S., Munch, J.C., Papen, H., Priesack, E., Schmid, H.P., Steinbrecher, R., Rosenbaum, U., Teutsch, G., Vereecken, H., 2011. A Network of Terrestrial Environmental Observatories in Germany. Vadose Zo. J. 10, 955–973. https://doi.org/10.2136/vzj2010.0139.

Zhang, X.L., Zhang, Q., Werner, A.D., Tan, Z.Q., 2017. Characteristics and causal factors of hysteresis in the hydrodynamics of a large floodplain system: Poyang Lake (China). J. Hydrol. 553, 574–583. https://doi.org/10.1016/j.jhydrol.2017.08.027.

Zimmer, M.A., Pellerin, B., Burns, D.A., Petrochenkov, G., 2019. Temporal Variability in Nitrate-Discharge Relationships in Large Rivers as Revealed by High-Frequency Data. Water Resour. Res. 55, 973–989. https://doi.org/10.1029/2018wr023478.

Zimmermann, B., Elsenbeer, H., De Moraes, J.M., 2006. The influence of land-use changes on soil hydraulic properties: Implications for runoff generation. For. Ecol. Manage. 222, 29–38. https://doi.org/10.1016/j.foreco.2005.10.070.